

Phase transitions of extended-range probabilistic cellular automata with two absorbing states

Franco Bagnoli*

*Dipartimento di Energetica, Università di Firenze,
Via S. Marta 3, 50139 Firenze, Italy*

Fabio Franchi†

*Centro Interdipartimentale per lo Studio delle Dinamiche Complesse (CSDC),
Università di Firenze,
Via Sansone 1, 50019 Sesto Fiorentino, Italy*

Raúl Rechtman‡

*Centro de Investigación en Energía,
Universidad Nacional Autónoma de México,
Apdo. Postal 34, 62580 Temixco, Mor., Mexico*

(Dated: December 31, 2018)

We study phase transitions in a long-range one-dimensional cellular automaton with two symmetric absorbing states. It includes and extends several other models, like the Ising and Domany-Kinzel ones. It is characterized by a competing ferromagnetic linear coupling and an antiferromagnetic non-linear one. Despite its simplicity, this model exhibits an extremely rich phase diagram. We present numerical results and mean-field approximations.

PACS numbers: 68.35.Rh,64.60.-i,05.50.+q

I. INTRODUCTION

Simple discrete models are valuable tools for exploring phase transitions, both in equilibrium and out of equilibrium. A paradigmatic example of the first kind is the kinetic Ising model (heat-bath dynamics), which can be formulated as a Probabilistic Cellular Automaton (PCA) (see Appendix and Ref. [1]). One of the simplest examples of a system exhibiting out of equilibrium phase transitions is the Domany-Kinzel (DK) model [2], which is a natural extension of the directed percolation (DP) problem in the language of cellular automata.

Frustrations play a central role in characterizing the phase diagrams of many simple models. One can have geometric frustrations, like in a triangular antiferromagnetic Ising model, or fluctuating coupling, like in spin glasses [3] or p-spin [4] models. For instance, in the p-spin model, the character (ferro or anti-ferro) of the interaction varies widely with the local magnetization (i.e. even a flip of a single spin may invert the interaction). We discuss here a simpler one dimensional model in which frustrations play a central role. This model is a variation of the droplet model in which the particles tend to repel each other when they are dispersed but in which clusters, once formed, cannot break and only particles near

the surface can eventually leave them.

The model originated from the schematization of the mechanism of opinion formation in a homogeneous (no leader) society [5], in which it was assumed that a coherent local community exerts a very strong social pressure on an individual's opinion. However, there is the possibility of disagreement with a weak local majority depending on the individual's education. In the case of a diffuse non-conformistic attitude, people tend to act in the opposite way of the local majority (antiferromagnetic coupling), introducing frustrations. The presence of absorbing states may cause the formation of large coherent clusters, whose interactions give way to interesting patterns.

This model could also be applied to a system of charged, magnetized metallic particles. These repel each other due to their charge, but are attracted due to their magnetic coupling. With a proper choice of parameters, one may have repulsion when particles are scattered. However, once a cluster of particles in contact appears, the mobility of charges may lower the electric field among this cluster and an external particle, and the interaction may become attractive. Other examples can be found in aggregation models.

In what follows, we discuss a one dimensional spin model characterized by two coupling factors; one that behaves like the Ising (magnetic) coupling, i.e., for a given spin, grows linearly with the local field, and a *nonlinear term* that is very low for a weak local field, but grows quickly when the local field exceeds a certain threshold.

In one dimension, no true phase transition appears for finite-range and finite-strength coupling. On the other

*also INFN, sez. Firenze and CSDC; Electronic address: franco.bagnoli@unifi.it

†Electronic address: fabio@dma.unifi.it

‡Electronic address: rrs@cie.unam.mx

hand, models presenting absorbing states, like the DK one, do exhibit nonequilibrium phase transitions. The presence of absorbing states may be related to the divergence of some coupling, that becomes infinite (see Appendix and Ref. [1]). Thus, in our model, we simply assume a two-level nonlinear coupling: zero for local field below a given threshold (corresponding to the parameter Q in the following) and infinite otherwise. Thus, in total we have four parameters: the range R , the external magnetic field H and local coupling J like in the Ising model, and the threshold Q . We denote these models by RQ , indicating the range and the threshold, say $R3Q1$, $R5Q2$, ...

The model can also be discussed as a one dimensional probabilistic cellular automaton. In this guise, it may be considered an extension of the DK model, or, more precisely, of the $R3Q1$ model [6]. This model exhibits a richer phase diagram than the DK one, and we shall show that for $R \rightarrow \infty$, the RQ model presents novel features, like a disorder-chaotic transition.

It is not surprising that frustrations gives rise to disordered behavior, which may be sometimes considered chaotic from a microscopic point of view. We investigate this aspect using an original chaotic observable, corresponding to a finite-distance Lyapunov exponent. However, when renormalized (or locally averaged), a “disordered” behavior simply corresponds to a stable almost-zero magnetization. In the mean-field approximation, it corresponds to a fixed point of observables. In our model also a coherently-chaotic phase appears, in which large patches of sites oscillate widely, corresponding to a chaotic map in the mean-field approximation.

In summary, we observe that the *usual* transitions from ordered into active phases becomes much richer, being preceded by a transition from coherently chaotic to simply chaotic, then to more irregular states, the appearance of a parameter-insensitive disordered phase and finally an “escape” to ordered (quiescent) states with a discontinuous (first-order) character. The origin of this behavior is the competition between “linear” antiferromagnetic and “nonlinear” ferromagnetic couplings.

The paper is organized as follows. In Sec. II we present the RQ model both as a spin system and a PCA. In Sec. III we present numerical results of the model beginning with a review of the simplest non trivial case $R = 3$, $Q = 1$ and Sec. IV is devoted to a mean field discussion of the model. The paper ends with some conclusions.

II. THE MODEL

Both the kinetic Ising model (see Appendix) and the DK one are Boolean, one dimensional, $R = 2$ PCA in which the state of a given cell depends probabilistically on the sum S of the states of its two nearest neighbors at the previous time step. That is, there are three different conditional probabilities, $\tau(1|S)$, $S = 0, 1, 2$ that the future state of the cell is 1 given S neighbors in state

1. In the DK model $\tau(1|0) = 0$ which means that there is an absorbing phase corresponding to the configuration where the state on every cell is zero. The presence of more than one absorbing state can induce different behaviors and trigger the appearance of universality classes different from the usual directed percolation (DP) one [7–9].

We denote by $s_i^t \in \{0, 1\}$ the state at site $i = 0, \dots, L-1$ and time $t = 0, 1, \dots$. All operations on spatial indices are assumed to be modulo L (periodic boundary conditions). The range of interactions is denoted by R , that is, s_i^{t+1} depends on the states at time t in a neighborhood \mathcal{N}_i that contains the R nearest neighbors of site i . It is convenient to introduce also the spin notation: $\sigma_i^t = 2s_i^t - 1$, $\sigma_i^t \in \{-1, 1\}$.

The spin σ_i^t “feels” the local field $V(m_i^t) = H + [J + K(m_i^t)]m_i^t$, where H is an external field, J a coupling constant and the local magnetization is defined as

$$m_i^t = \sum_{j \in \mathcal{N}_i} \sigma_j^t = 2S_i^t - R,$$

where

$$S_i^t = \sum_{j \in \mathcal{N}_i} s_j^t.$$

The presence of absorbing states is due to the nonlinear coupling K given by

$$K(m) = K(m(S, R), Q) = \begin{cases} -k & \text{if } S < Q, \\ k & \text{if } S > R - Q, \\ 0 & \text{otherwise.} \end{cases}$$

with k a constant. This term is relevant only if it is dominant with respect to the linear one. We thus choose the limit $k \rightarrow \infty$, so that the transition probabilities $\tau(1|S)$ are given by

$$\tau(1|S) = \begin{cases} 0 & \text{if } S < Q, \\ 1 & \text{if } S > R - Q, \\ \frac{1}{1 + \exp\{-2[H + Jm(S, R)]\}} & \text{otherwise.} \end{cases} \quad (1)$$

For $Q = 0$ we recover the usual heat-bath dynamics for an Ising-like model with reduced Hamiltonian $\mathcal{H} = \sum_i V(m_i)\sigma_i$. For $R = 3$, $Q = 1$ we have the model of Ref. [6] with two absorbing states. The quantities H and J range from $-\infty$ to ∞ . For easy plotting, we use $j = [1 + \exp(-2J)]^{-1}$ and $h = [1 + \exp(-2H)]^{-1}$ as control parameters, mapping the real axis $(-\infty, \infty)$ to the interval $[0, 1]$.

The fraction c of ones in a configuration and the concentration of clusters ρ are defined by

$$c = \frac{1}{L} \sum_i s_i \quad \text{and} \quad \rho = \frac{1}{L} \sum_i |s_i - s_{i+1}|.$$

Both the uniform zero-state and one-state correspond to $\rho \rightarrow 0$ in the thermodynamic limit, while the active state corresponds to $\rho > 0$.

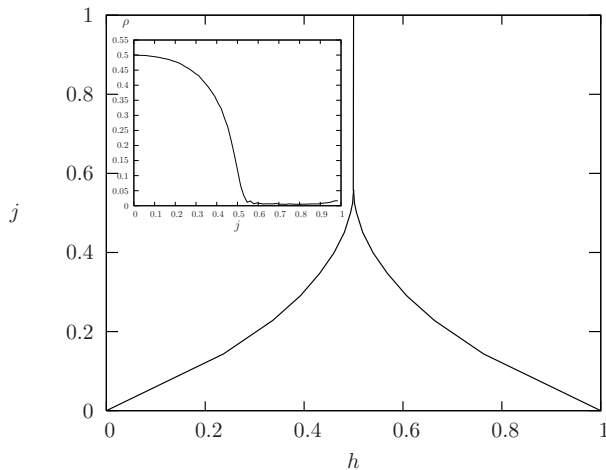


FIG. 1: Phase diagram of $R3Q1$ model. The upper-left region corresponds to the absorbing state 0, the upper-right region to the absorbing state 1 and the lower region to the disordered phase. In the inset we show the asymptotic value of ρ as a function of j for $H = 0$ ($h = 0.5$).

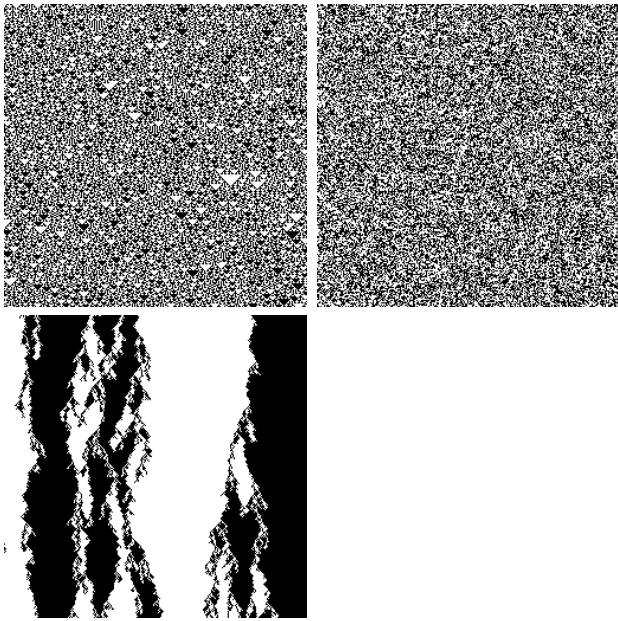


FIG. 2: Typical space time patterns of the $R3Q1$ model for $H = 0$ ($h = 0.5$) with $L = 256$. (A – top left) Chaotic deterministic pattern $j = 0.03125$. (B – top right) Disordered phase $j = 0.5$. (C – bottom left) competition between quiescent phases $j = 0.54688$ (first-order transition).

III. NUMERICAL RESULTS

Let us first review the $R3Q1$ case, whose phase diagram is reported in Fig. 1. A first order phase transition occurs on the vertical line that ends at a bicritical point where it meets two second order phase transition curves. In the neighborhood of the first order phase transition line a typical pattern of the system is composed by large

patches of zeroes and ones, separated by disordered zones (walls) whose width does not grow in time. These walls perform a sort of random motion and annihilate in pairs (see Fig. 2-C). By lowering J an active, disordered phase appears (see Fig. 2-B). The transition between the ordered (absorbing) and disordered (active) phases occurs by destabilization of the width of the walls, that percolate in the whole system. In the limit $J = -\infty$ ($j = 0$) we have typical “chaotic” class-3 cellular automata patterns [10], as shown in Fig. 2-A. Damage spreading analysis [6] show that inside the active phase there is a region in which a variation in the initial configuration can influence the asymptotic configuration. This region may be called chaotic. However, in the mean field approximation, this region simply corresponds to a stable fixed point of the average density. Indeed, the fluctuations of the density remains quite small and a spatial coarse-graining would generate a simple random pattern.

This underlining “disorder” is revealed also by the asymptotic value of ρ for $H = 0$ ($h = 0.5$) as a function of j , shown in the inset of Fig. 1. It exhibits a monotonic behavior, with a maximum for $j = 0$ (corresponding to the smallest average length of homogeneous clusters) and a continuous phase transition at the bicritical point, that separates the active ($\rho > 0$) and quiescent ($\rho = 0$) phases.

By increasing R , new features appear. Typical patterns are shown in Fig. 3 for different values of j . As illustrated in Fig. 4, ρ is no longer a monotonic function of j , and a new, *less disordered* region appears inside the active one for small values of j . The transition between the active and the quiescent phases become sharper with increasing R , as shown in Fig. 4.

The pattern shown in Fig. 3-a is reminiscent of “chaotic” deterministic cellular automata. We refer to this region as *coherently-chaotic*, since it corresponds to “irregular” coherent oscillations of large patches of sites. This region of the parameters is dominated by an almost-deterministic behavior, and the presence of many metastable “absorbing” states, revealed by transient regular patterns in Fig. 3-a. As we discuss in Sec. IV, the mean field analysis gives a chaotic map for large anti-ferromagnetic values of J , but we were unable to find a clear order parameter that numerically distinguishes this region from the broader “chaotic” one in which the asymptotic configuration exhibits a dependence on variations in the initial configuration. In Sec. III A, we analyze the chaotic region by means of (finite size) Lyapunov exponents.

By increasing J , the coherent patches shrink and the Lyapunov exponent decreases and finally becomes negative. The system asymptotically loses its dependence on the initial conditions and is dominated by the stochastic components. This phase is termed *irregular*, and appears completely random. Fig. 3-b shows a typical pattern at the boundary between the chaotic and the irregular phase.

Our simulations were carried out using the fragment method [11], in which a set of configurations (replicas)

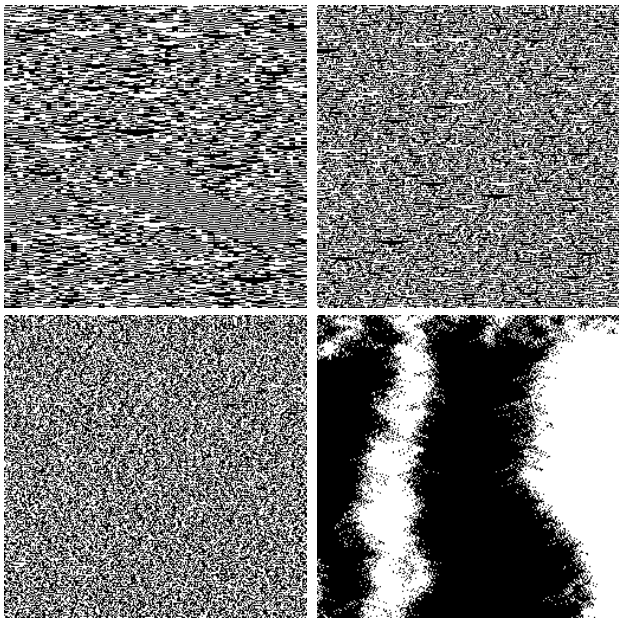


FIG. 3: Typical space time patterns ($L = 256$) for model $R11Q1$ and $H = 0$, starting from a disordered initial condition with $\rho_0 = 0.5$. (A) [top left, $j = 0.056250$]: “coherently-chaotic” phase. One can observe rare “triangles” with “base” larger than R , corresponding to the unstable absorbing states, and other metastable patterns, corresponding to additional absorbing states for $J \rightarrow -\infty$. (B) [top right, $j = 0.421875$]: At the boundary between the chaotic and the irregular phase, the only locally absorbing states are (rare) patches of 0 and 1. Most of the pattern looks random, with some “triangles” reminiscent of chaotic CA. (C) [bottom left, $j = 0.478125$]: Disordered phase. the pattern looks random and the difference between patterns obtained with different values of the parameters (and the same random numbers) is vanishing. (D) [bottom right, $j = 0.562500$]: Quiescent phase. In this phase the only stable states are the absorbing ones. The boundaries separating the phases move randomly until coalescence.

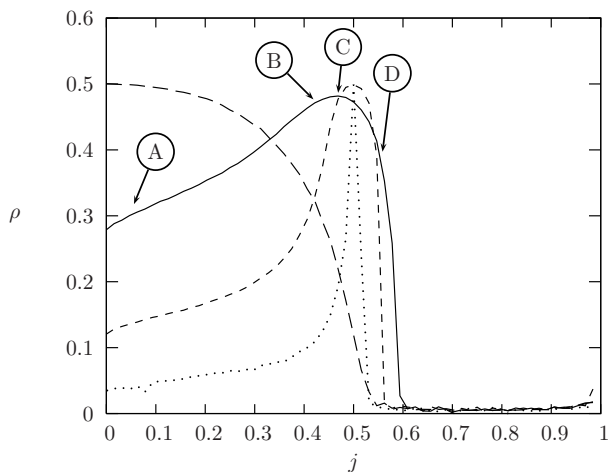


FIG. 4: Behavior of ρ for $H = 0$. $R3Q1$ (long dashed), $R11Q1$ (solid), $R41Q1$ (dashed) and $R81Q1$ (dotted). Letters correspond to patterns in Fig. 3.

are updated with different values of parameters using the same random numbers, and the same initial configuration.

By observing in rapid sequence the patterns generated with increasing values of J , one observes a sudden “freezing” of the (random) image, just before the transition between the active to quiescent phases, corresponding to Fig. 3-c. This effect is due to the insensitivity of the patterns not only to the initial condition, but also to the parameters, see Sec III B. We term this phase *disordered*.

Finally, the quiescent phase is asymptotically dominated by the two absorbing states, with the usual annihilating walls dynamics, Fig. 3-d.

Fig. 4 shows that the active-quiescent transition becomes sharper when R is increased, and that the cluster density exhibits a cusp at the transition. By enlarging this region one sees that for $H = 0$ (Fig. 5) the cluster density exhibits two sharp bends, while for $H = 0.42$, (Fig. 6), only one bend is present. This is reminiscent of the universality class change (parity conservation, DP) for $H = 0$, $H \neq 0$, respectively, in the $R3Q1$ model [6]. Notice also that the irregular–disorder transition at $j \simeq 0.494$ is rather peculiar, since ρ first decreases and then suddenly jumps to high values.

The bends are not finite size or time effects. As shown in Fig. 3-c, in this range of parameters the probability of observing a local absorbing configuration (i.e. patches of zeroes or ones) is vanishing. All other local configurations have finite probability of originating zeroes or ones in the next time step. The observed transitions are essentially equivalent to those of an equilibrium system, that in one dimension and for short-range interactions cannot exhibit a true phase transition. The bends thus become real salient points only in the limit $R \rightarrow \infty$.

A. Chaos and Lyapunov exponent in cellular automata

State variables in cellular automata are discrete, and thus the usual linear stability analysis classifies them as stable systems. The occurrence of disordered patterns and their propagation in stable dynamical systems can be classified into two main groups: *transient chaos* and *stable chaos*.

Transient chaos is an irregular behavior of finite lifetime characterized by the coexistence in the phase space of stable attractors and chaotic non attracting sets, namely chaotic saddles or repellers [12]. After a transient irregular behavior, the system generally collapses abruptly onto a non-chaotic attractor. This kind of behavior is reminiscent of some *class-4* (nonchaotic) deterministic cellular automata (DCA) [10], and can be present in continuous systems having a discrete dynamics as a limiting case [13].

Stable chaos constitutes a different kind of transient irregular behavior [14, 15] which cannot be ascribed to the presence of chaotic saddles and therefore to diver-

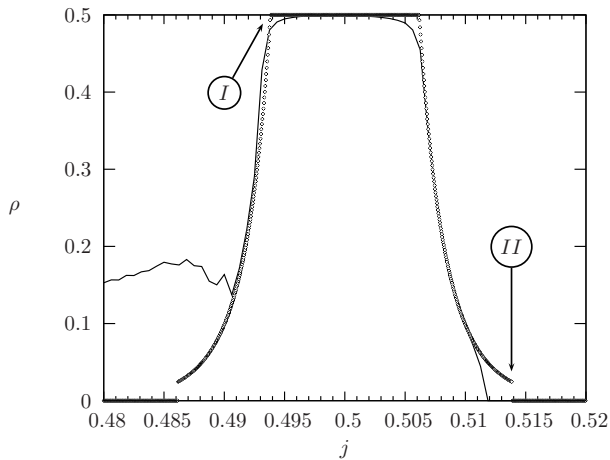


FIG. 5: Comparisons between numerical (thin line) and mean-field (thick, dotted line) results for $R81Q1$ and $H = 0$ ($h = 0.5$). The estimated critical values are $j_I^* \simeq 0.493827$ and $j_{II}^* \simeq 0.51384$. This figure has been obtained with much larger simulations of the corresponding line in Fig. 4, and more details emerge. The patterns shown in Fig. 3 (which however refer to $R = 11$) illustrate the typical behavior of the system to the left (B), in the middle (C) and to the right (D) of the plateau.

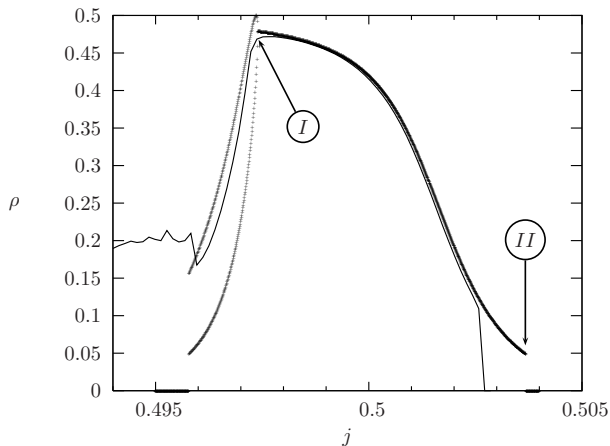


FIG. 6: Comparisons between numerical (thin line) and mean-field (thick, dotted line) results for $R201Q5$ and $H = 0.42$ ($h = 0.7$). The two set of pluses mark the period-two region. The estimated critical values are $j_I^* \simeq 0.49740$ and $j_{II}^* \simeq 0.50369$.

gence of nearby trajectories. Moreover, the lifetime of this transient regime may scale exponentially with the system size (supertransients as defined in Refs. [14, 15]), and the final stable attractor is practically never reached for large enough systems. One is thus allowed to assume that such transients may be of substantial experimental interest and become the only physically relevant states in the thermodynamic limit.

The emergence of this “chaoticity” in *class-3* (chaotic) DCA dynamics, is effectively illustrated by the damage spreading analysis [16, 17], which measures the sensitiv-

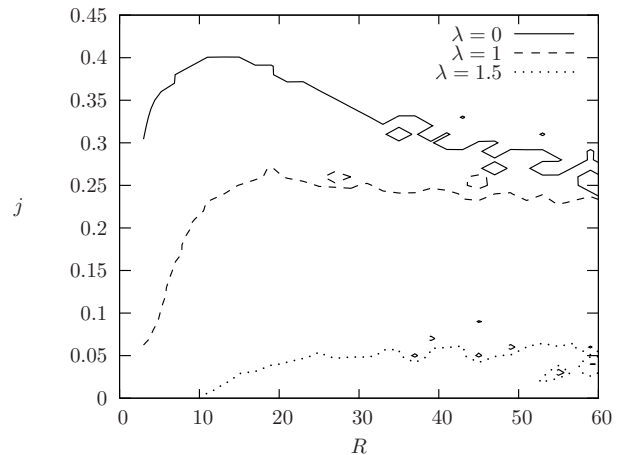


FIG. 7: Contour plot of the maximum Lyapunov λ exponents for different values of R and j , for $H = 0$. The solid line represent the boundary between the $\lambda \geq 0$ phase and the $\lambda = -\infty$ one.

ity to initial conditions and for this reason is considered as the natural extension of the Lyapunov technique to discrete systems. In this method, indeed, one monitors the behavior of the distance between two replicas of the system evolving from slightly different initial conditions, or the speed of propagation of a disturbance [18]. The dynamics is considered unstable and the DCA is called chaotic, whenever a small initial difference between replicas spreads through the whole system. On the contrary, if the initial difference eventually freezes or disappears, the DCA is considered non chaotic.

Due to the limited number of states of the automaton, damage spreading does not account for the maximal “production of uncertainty”, since the two replicas may synchronize locally just by chance (self-annihilation of the damage). Moreover, there are different definitions of damage spreading for the same rule [19].

To better understand the nature of the active phase, and up to what extent it can be denoted *chaotic*, we extend the finite-distance Lyapunov exponent definition [20] to probabilistic cellular automata. A similar approach has been used in Ref. [21], calculating the Lyapunov exponents of a Kauffman random Boolean network in the annealed approximation. As shown in this latter paper, this computation gives the value of the (classic) Lyapunov exponent obtained by the analysis of time-series data using the Wolf algorithm [22].

Given a Boolean function $f(x, y, \dots)$, we define the Boolean derivative $\partial f / \partial x$ with respect to x by

$$\frac{\partial f}{\partial x} = \begin{cases} 1 & \text{if } f(|x-1|, y, \dots) \neq f(x, y, \dots), \\ 0 & \text{otherwise,} \end{cases} \quad (2)$$

which represents a measure of sensitivity of a function with respect to x . The evolution rule of a probabilistic

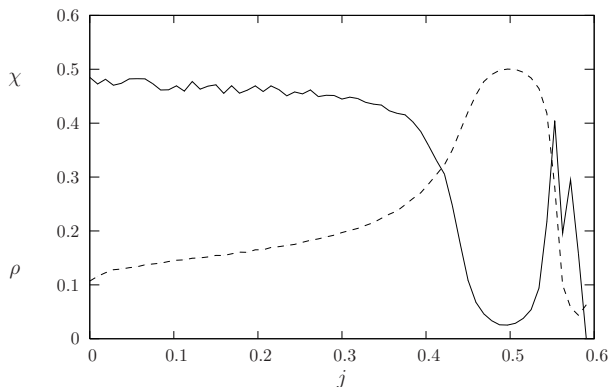


FIG. 8: Susceptibility χ (continuous line) and average number of clusters ρ (dashed line) for $R11Q1$, $H = 0$, $\Delta j = 0.01$

cellular automaton can be written as

$$x_i^{t+1} = \begin{cases} 1 & r < \tau(1|S_i^t), \\ 0 & \text{otherwise} \end{cases}$$

where r is a random number uniformly distributed in $[0, 1]$. The Boolean derivative with respect to x_j is evaluated by using the same r in the comparison implied in Eq. (2).

For a PCA, we can thus build the Jacobian matrix $J_{ij} = \partial x_i^{t+1} / \partial x_j^t$, $i, j = 0, \dots, L - 1$. The maximum Lyapunov exponent λ can now be defined in the usual way as the expansion rate of a tangent vector $\mathbf{v}(t)$, whose time evolution is given by

$$\mathbf{v}(t+1) = \mathbf{J}\mathbf{v}(t).$$

When all the components of \mathbf{v} become zero, $\lambda = -\infty$ and no information about the initial configuration may “percolate” as $t \rightarrow \infty$ [20]. This maximum Lyapunov exponent is also related to the synchronization properties of cellular automata [23].

A preliminary numerical computation of λ for our model is reported in Fig. 7. It can be noticed that the boundary $j_c(R)$ of $\lambda \geq 0$ is not monotonic with R , reaching a maximum value for $R \simeq 11$. By comparisons with Fig. 4, one can see that the chaotic phase is included in the irregular one.

B. Parameter dependence

We can numerically characterize the irregular-disorder transition by looking at the sensitivity of space-time patterns with respect to the variations of parameters. Using the fragment method [11] a set of configurations (replicas) are updated with different values of parameters using the same random numbers, i.e. with the same disordered field and initial conditions. The quantity

$$\chi(J) = \lim_{\Delta j \rightarrow 0} \lim_{t \rightarrow \infty} \sum_i |s_i^t(J + \Delta J) - s_i^t(J)|$$

is a measure of the susceptibility. For large correlations one expects very small differences among replicas. As shown in Fig. 8, this susceptibility is strongly correlated to the average number of clusters ρ .

IV. MEAN FIELD APPROXIMATION

In the simplest mean field approximation, the density c evolves in time according to

$$c(t+1) = \sum_{S=0}^R W^{(R,S)}(c(t)) \tau(1|S), \quad (3)$$

with

$$W^{(R,S)}(c) = \binom{R}{S} c^S (1-c)^{R-S}.$$

An example of a mean-field phase diagram is reported in Fig. 9.

For large R , $W^{(R,S)}$ can be approximated by

$$W^{(R,S)}(c) \simeq \frac{1}{\sqrt{2\pi c(1-c)R}} \exp\left[-\frac{R(S/R - c)^2}{2c(1-c)}\right], \quad (4)$$

and the summation can be replaced by an integral. The parameters of the resulting equation may be rescaled by using $\tilde{J} = JR$ and $\tilde{Q} = Q/R$. In the limit $R \rightarrow \infty$ (\tilde{J} and \tilde{Q} fixed), $c(t+1) = f(c(t); H, \tilde{J})$ with

$$f = \begin{cases} 0 & \text{if } c < \tilde{Q}, \\ 1 & \text{if } c > 1 - \tilde{Q}, \\ \frac{1}{1 + \exp(-2(H + \tilde{J}(2c - 1)))} & \text{otherwise.} \end{cases} \quad (5)$$

The requirement of constant rescaled variables means that the variations of J for large R triggers large variations of \tilde{J} , and consequently the transition region becomes sharper.

This approximation is supposed to be particularly good in the disordered phase, i.e. for $J, H \simeq 0$, as shown in Fig. 5. In the finite-dimensional case, one has to add a noise term, representing the influence of neighboring sites, whose amplitude is of the order of the width of the Gaussian in Eq. (4), $\sqrt{c(1-c)/R}$.

In this mean-field approximation, the order parameters c and the numerical density of clusters ρ are related by $\rho = 2c(1-c)$.

For $J, H \simeq 0$ the mean field approximation gives a stable fixed point $c^*(H, \tilde{J}) \neq 0, 1$ for the density, which assumes the maximum value $c^* = 0.5$ for $J = H = 0$.

The origin of the irregular-disordered and disorder-quiet phase transitions marked by (I) and (II) respectively in Figs. 5 and 6 is due to the loss of stability of the mean-field fixed point $c^* \neq 0, 1$ (see Eq. (5) and Fig. 10).

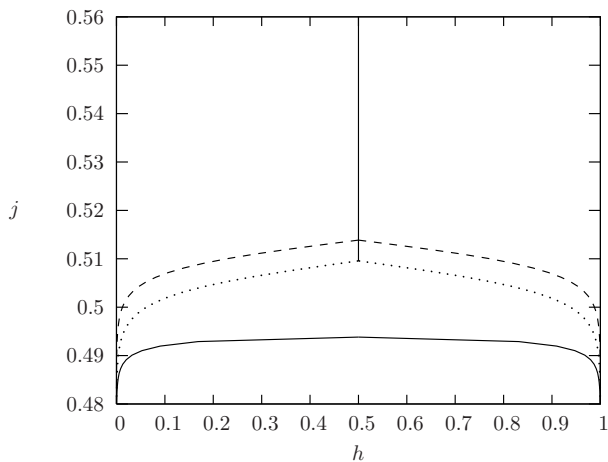


FIG. 9: Mean-field phase diagram for $R = 81$. The upper curves correspond to the transition II from the quiescent to the disordered phases, $R81Q5$ (dashed) and $R81Q1$ (dotted). The solid curve corresponds to the transition I from the disordered to the irregular phase.

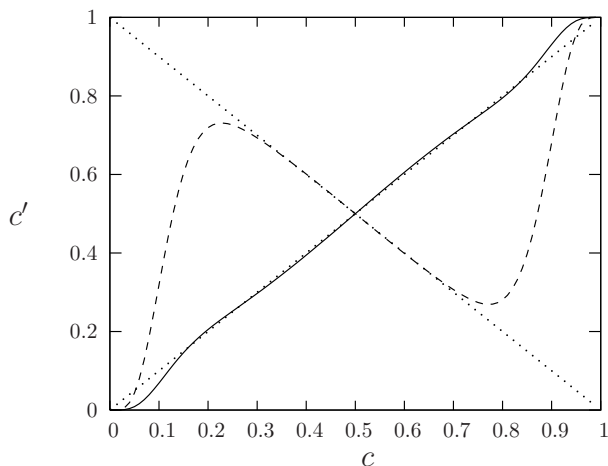


FIG. 10: Mean field map Eq. (3) in the neighborhood of transition I ($\tilde{J} \simeq -1$, dashed line) and II ($\tilde{J} \simeq 1$, solid line), for $H = 0$ and $\tilde{Q} = 0.02$

The transition I is given by

$$c_{\text{I}}^* = f(c_{\text{I}}^*; H, \tilde{J}); \quad \left. \frac{df(c; H, \tilde{J})}{dc} \right|_{\text{I}} = -1. \quad (6)$$

which would induce a period-doubling cascade in the mean-field approximation (disregarding the presence of absorbing states). The solution of Eq. (6) is

$$c_{\text{I}}^* = \frac{1}{2} \left(1 + \sqrt{1 + \tilde{J}^{-1}} \right),$$

$$H_{\text{I}}^* = -\tilde{J} \sqrt{1 + \tilde{J}^{-1}} - \frac{1}{2} \log \left(\frac{1 - \sqrt{1 + \tilde{J}^{-1}}}{1 + \sqrt{1 + \tilde{J}^{-1}}} \right).$$

The critical value J_{I}^* can be obtained numerically once given the value of $H^* = H^*(J^*)$, and corresponds to the left bend in Fig. 5 and 6.

For $H = 0$ (Fig. 5) the period-doubling instability brings the local configuration into an absorbing state, and the lattice dynamics is therefore driven by interactions among patches which are locally absorbing. This essentially corresponds to the dynamics of a Deterministic Cellular Automata (DCA) of *chaotic* type, i.e. a system which is insensitive to infinitesimal perturbations but reacts in an unpredictable way to *finite* perturbations [13]. In other words, in this region the original stochastic model behaves like a “chaotic” deterministic one after a coarse-graining of patches. We expect that this correspondence will become more and more exact with growing R . From a theoretic-field point of view this means that the renormalization flux tends towards a “chaotic” model instead of the usual fixed-point dynamics.

For $H = 0.42$, as shown in Fig. 6, the period-two phase has a finite amplitude, before falling into the DCA-like dynamics by reducing J .

For $J > 0$ (transition II) we have

$$c_{\text{II}}^* = f(c_{\text{II}}^*; H, \tilde{J}) = \begin{cases} \tilde{Q} \\ 1 - \tilde{Q} \end{cases}$$

and thus the critical value J_{II}^* is

$$J_{\text{II}}^* = \frac{1}{2\tilde{Q} - 1} \left[\pm H + \frac{1}{2} \log \left(\frac{\tilde{Q}}{1 - \tilde{Q}} \right) \right].$$

Once that a portion of the lattice has been attracted to an absorbing state, it pulls the neighboring regions to this same state, due to the ferromagnetic ($J > 0$) coupling.

This approximation, disregarding fluctuations, overestimates the critical value J_{II}^* , as shown in Figs. 5 and 6.

We analyze extensively the mean-field behavior of the system for $H = 0$ and $J = -\infty$. As shown in Fig. 11, for a given value of R , there is always a critical Q_c value of Q for which the active phase disappears, with an approximate correspondence $Q_c \simeq 2/5R$. One can also observe that the chaotic oscillations of the mean-field map, that roughly corresponds to the coherent-chaotic phase of the model, appear only for large values of R . Since the absorbing states are always present, these chaotic oscillations may bring the system into the quiescent phase, as shown by the “hole” to the right of triangles in Fig. 11.

The correspondence between the chaotic behavior of the mean-field approximation and the actual behavior of the system will be the subject of a future work.

V. CONCLUSIONS

We have investigated a general one dimensional model with extended-range interactions and symmetric absorbing states. The model is characterized by a competing ferromagnetic linear coupling and an antiferromagnetic nonlinear one.

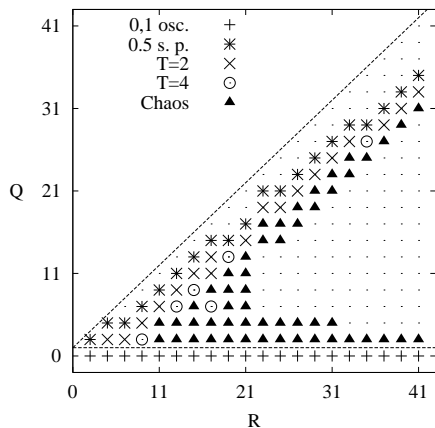


FIG. 11: Case $H = 0$, $J = -\infty$: the mean-field $R - Q$ phase diagram of the mean-field approximation. Points mark parameter values for which the absorbing states are the only stable attractors. A plus sign denotes period-2 temporal oscillations between absorbing states, a star denotes the presence of a stable point at $c = 0.5$, a cross (circle) denotes period-two (four) oscillations between two non-zero and non-one densities, triangles denote chaotic oscillations.

By means of numerical simulations and mean field approximations we have shown that a chaotic phase is present for strong antiferromagnetic coupling. This phase may be identified as a stable-chaotic region, in which the behavior of the (originally stochastic) system is essentially deterministic and its behavior is highly irregular and essentially unpredictable. The mean field map exhibit a chaotic behavior for a large interaction range R , and this behavior is reflected in the appearance of many metastable states in the system, for extremely strong antiferromagnetic coupling.

A disordered phase, insensitive of parameter variations, appears at the boundary between the active and the quiescent ones, and the transitions appear to be of equilibrium type, i.e. truly salient points only in the limit $R \rightarrow \infty$.

We expect that in higher dimensions one can recover some aspects of these phase transitions without imposing the presence of absorbing states, i.e. using finite couplings.

Acknowledgements

Partial economic support from project IN109602 DGAPA-UNAM and the Coordinaci3n de la Investigaci3n Científica UNAM is acknowledged.

APPENDIX A: EQUIVALENCE BETWEEN DYNAMIC ISING MODEL AND CELLULAR AUTOMATA

As an illustration, we present here a derivation of the equivalence of the kinetic Ising model (here we choose heat bath) with a cellular automaton (the Domany-Kinzel model) in order to elucidate the role of infinite coupling parameters and absorbing states. This derivation is similar to that of Ref. [1] but more general.

The Ising model is defined by the couplings among spins. The configuration at time t is denoted as $\sigma = \sigma_1, \sigma_2, \dots$ and the configuration at time $t + 1$ as $\sigma' = \sigma'_1, \sigma'_2, \dots$. Let us write the temperature-dependent Hamiltonian as

$$\mathcal{H}(\sigma) = \sum_i H(\sigma_{i-1}, \sigma_i \sigma_{i+1}),$$

with

$$H(x, w, y) = J^{(0)}w + J^{(1)}xw + J^{(2)}wy + J^{(3)}xwy. \quad (\text{A1})$$

The transition probabilities τ must obey the detailed balance condition

$$\frac{\tau(\sigma'|\sigma)}{\tau(\sigma|\sigma')} = \exp(\mathcal{H}(\sigma') - \mathcal{H}(\sigma)).$$

In each step we can update in parallel all even or odd sites, obtaining

$$\frac{\tau(\sigma'|\sigma)}{\tau(\sigma|\sigma')} = \prod_i \frac{\tau(\sigma_{i-1}, \sigma'_i, \sigma_{i+1}|\sigma_{i-1}, \sigma_i, \sigma_{i+1})}{\tau(\sigma_{i-1}, \sigma_i, \sigma_{i+1}|\sigma_{i-1}, \sigma'_i, \sigma_{i+1})},$$

where the product is restricted to either even or odd sites. The detailed balance condition can thus be satisfied locally. Choosing the Heat Bath dynamics

$$\tau(x, 1, y|x, w, y) = \frac{\exp(-H(x, 1, y))}{\exp(-H(x, -1, y)) + \exp(-H(x, 1, y))}$$

the transition probabilities does not depend on the present value of the spin $w = \sigma_i^t$ so that the lattice (with even or infinite lattice sites) may be decoupled into two noninteracting sublattices with the same geometry of the DK model. From now on, to be coherent with the usual cellular automaton notation, we shall express the transition probabilities in terms of the Boolean variables $s_i = (\sigma_i + 1)/2$, and we shall denote the local field as $h(a, b) \equiv H(2a - 1, 1, 2b - 1)$.

Let us denote the DK transition probabilities $\tau(s'_i|s_{i-1}, s_{i+1})$ as

$$\tau(1|00) = \varepsilon, \quad \tau(1|01) = \tau(1|10) = p, \quad \tau(1|11) = q.$$

We get for the heat bath dynamics

$$\tau(1|ab) = \frac{1}{1 + \exp(-2h(a, b))}$$

and thus

$$h(a, b) = \frac{1}{2} \ln \frac{\tau(1|ab)}{1 - \tau(1|ab)}.$$

Substituting into Eq. (A1) one obtains a linear system

$$\begin{aligned} J^{(0)} - J^{(1)} - J^{(2)} + J^{(3)} &= \frac{1}{2} \ln \frac{\varepsilon}{1 - \varepsilon}, \\ J^{(0)} + J^{(1)} - J^{(2)} - J^{(3)} &= \frac{1}{2} \ln \frac{p}{1 - p}, \\ J^{(0)} - J^{(1)} + J^{(2)} - J^{(3)} &= \frac{1}{2} \ln \frac{p}{1 - p}, \\ J^{(0)} + J^{(1)} + J^{(2)} + J^{(3)} &= \frac{1}{2} \ln \frac{q}{1 - q}. \end{aligned}$$

Finally, we have

$$\begin{aligned} J^{(0)} &= \frac{1}{8} \ln \frac{\varepsilon}{1 - \varepsilon} + \frac{1}{8} \ln \frac{q}{1 - q} + \frac{1}{4} \ln \frac{p}{1 - p}, \\ J^{(1)} = J^{(2)} &= -\frac{1}{8} \ln \frac{\varepsilon}{1 - \varepsilon} + \frac{1}{8} \ln \frac{q}{1 - q}, \\ J^{(3)} &= \frac{1}{8} \ln \frac{\varepsilon}{1 - \varepsilon} + \frac{1}{8} \ln \frac{q}{1 - q} - \frac{1}{4} \ln \frac{p}{1 - p}. \end{aligned}$$

In the limit $\varepsilon \rightarrow 0$ all couplings become infinite.

-
- [1] A. Georges and P. Le Doussal, J. Stat. Phys. **54**, 1011 (1989).
- [2] E. Kinzel and W. Domany, Phys. Rev. Lett. **53** (1984); W. Kinzel, Z. Phys. B **58** (1985); W. Kinzel, in *Percolation Structures and Processes*, G. Deutsch, R. Zallen and J. Adler, editors (Adam Hilger, Bristol, 1983).
- [3] M. Mézard, G. Parisi, and M. A. Virasoro, *Spin Glass Theory and Beyond* (World Scientific, Singapore, 1987); K.H. Fischer and J.A. Hertz, *Spin Glasses* (Cambridge University Press, Cambridge, England, 1991).
- [4] D.J. Gross and M. Mézard, Nucl. Phys. **B240**, 431 (1984); E. Gardner, *ibid.* **B257**, 747 (1985).
- [5] F. Bagnoli, F. Franci and R. Rechtman, in *Cellular Automata*, S. Bandini, B. Chopard and M. Tomassini (editors), (Springer-Verlag, Berlin 2002) p. 249.
- [6] F. Bagnoli, N. Boccara and R. Rechtman, Phys. Rev. E **63**, 46116 (2001).
- [7] H. Hinrichsen, Phys. Rev. E **55**, 219 (1997).
- [8] H. K. Janssen, Z. Phys. B **42**, 152 (1981).
- [9] P. Grassberger, Z. Phys. B **47**, 365 (1982).
- [10] S. Wolfram: Physica D **10**, 1 (1984).
- [11] F. Bagnoli, P. Palmerini and R. Rechtman, Phys. Rev. E **55**, 3970 (1997).
- [12] T. Tel, *Proceedings of the 19th IUPAP International Conference on Statistical Physics*, edited by Hao Bai-lin (World Scientific Publishing: Singapore 1996).
- [13] F. Bagnoli and R. Rechtman, Phys. Rev. E **59**, R1307 (1999); F. Bagnoli and F. Cecconi, Phys. Lett. A **260**, 9-17 (2001) and references therein.
- [14] J.P. Crutchfield and K. Kaneko, Phys. Rev. Lett. **60**, 2715 (1988), K. Kaneko, Phys. Lett. **149A**, 105 (1990).
- [15] A. Politi, R. Livi, G.-L. Oppo, and R. Kapral, Europhys. Lett. **22**, 571 (1993).
- [16] P. Grassberger, J. Stat. Phys. **79**, 13 (1995).
- [17] F. Bagnoli, J. Stat. Phys. **79**, 151 (1996).
- [18] S. Wolfram (Ed.) *Theory and Application of Cellular Automata* (Addison-Wesley, Reading, MA, 1986).
- [19] H. Hinrichsen, J. S. Weitz and E. Domany J. Stat. Phys. **88**, 617-636 (1997).
- [20] F. Bagnoli, R. Rechtman and S. Ruffo, Phys. Lett. A **172**, 34 (1992).
- [21] B. Luque and R.V. Solé, Physica A 284 (2000) 33-45
- [22] A. Wolf, JB Swift, HL Swinney, and JA Vastano, Physica D, **16**, 285 (1985).
- [23] F. Bagnoli and R. Rechtman, Phys. Rev. E **59**, R1307 (1999).